



# Core-Shell Structured Pt<sub>x</sub>Mo<sub>y</sub>@TiO<sub>2</sub> Nanoparticles Synthesized by Reverse Microemulsion for Methanol Electrooxidation of Fuel Cells

Tianyu Ai, Shuo Bao and Jinlin Lu\*

School of Materials and Metallurgy, University of Science and Technology Liaoning, Anshan, China

The high price of catalyst and poor durability still restrict the development of fuel cells. In this work, core-shell structured Pt<sub>x</sub>Mo<sub>y</sub>@TiO<sub>2</sub> nanoparticles with low Pt content are prepared by a reverse microemulsion method. The morphologies, particle size, structure, and composition of Pt<sub>x</sub>Mo<sub>y</sub>@TiO<sub>2</sub> nanoparticles are examined by several techniques such as X-ray Diffraction, X-ray photoelectron spectroscopy and transmission electron microscopy, etc. The Pt<sub>x</sub>Mo<sub>y</sub>@TiO<sub>2</sub> electrocatalysts show significantly higher catalytic activity and better durability for methanol oxidation than the commercial Pt/C (E-TEK). Compared to Pt/C catalyst, the enhancement of the electrochemical performance of Pt<sub>x</sub>Mo<sub>y</sub>@TiO<sub>2</sub> electrocatalysts can be attributed to the core-shell structure and the shift of the d-band center of Pt atoms, which can weaken the adsorption strength toward CO molecules, facilitate the removal of the CO groups and improve electrocatalytic activity. The development of Pt<sub>x</sub>Mo<sub>y</sub>@TiO<sub>2</sub> electrocatalysts is promising to reduce the use of noble metal Pt and has a great potential for application in fuel cells.

**Keywords:** reverse microemulsion method, PtMo alloy, core-shell structure, electrocatalyst, methanol oxidation reaction

## OPEN ACCESS

### Edited by:

Renheng Wang,  
Shenzhen University, China

### Reviewed by:

Chenyang Zhao,  
Shenzhen University, China  
Zhenjiang He,  
Central South University, China  
Feixiang Wu,  
Central South University, China

### \*Correspondence:

Jinlin Lu  
lujinlin@ustl.edu.cn

### Specialty section:

This article was submitted to  
Electrochemistry,  
a section of the journal  
Frontiers in Chemistry

**Received:** 14 February 2021

**Accepted:** 25 March 2021

**Published:** 30 April 2021

### Citation:

Ai T, Bao S and Lu J (2021) Core-Shell Structured Pt<sub>x</sub>Mo<sub>y</sub>@TiO<sub>2</sub> Nanoparticles Synthesized by Reverse Microemulsion for Methanol Electrooxidation of Fuel Cells. *Front. Chem.* 9:667754. doi: 10.3389/fchem.2021.667754

## INTRODUCTION

Direct methanol fuel cell (DMFC) is becoming more and more popular because of its abundant fuel sources, high energy density (6.09 Kwh Kg<sup>-1</sup>), environmental friendliness, high conversion, and low price (Zhao et al., 2011; Zhu et al., 2014; Lin et al., 2020). Due to the disadvantages of the platinum (Pt) group, such as high price, low yield, easy poisoning by oxidized intermediate products and poor durability, it is essential to design a new anode electrocatalyst with high-performance, low price, and high stability. So far, many efforts have been done to achieve the above goals. For example, various nanostructured architectures have been investigated including nanoframe, nanocrystal, nanowires, core-shell, and nanoclusters (Lang et al., 2016; Lu et al., 2016; Kwon et al., 2018; Oh et al., 2018; Liu et al., 2019). Among these nanostructures, core-shell structure is very special and has been widely used in electrocatalysis. Luo et al. (2008) synthesized core-shell structured Au@Pt and Fe<sub>3</sub>O<sub>4</sub>@Au@Pt nanoparticles by using a multiple steps method. The enhancement of catalytic performances for methanol oxidation reaction (MOR) was ascribed to the synergistic effect of oxide core and the shell surface. A core-shell structured Ag@Pt nanoparticle was prepared by the one step method using non-ionic surfactants (Li and Yamauchi, 2013). The activity enhancement is dependent on the adjustment of dendritic Pt shell with large surface area and the good anti-poisoning effect of the Ag core. The core-shell structured Pd@Pt nanoparticles

were synthesized using a one-step microwave heating method (Zhang et al., 2010). When Pd/Pt molar ratio was 1:3, the mass activity of Pd@Pt nanoparticles was six times higher than that of commercial Pt/C for MOR. Wang et al. (2019) synthesized PtFe@PtRuFe nanoparticles by using a multi-step solvent method. Due to the core-shell structure and surface alloying, the mass activity of the PtFe@PtRuFe catalysts was improved 1.68 times than that of state-of-the-art PtRu catalysts toward MOR. The core-shell structured Pd-Ni-Pt nanoparticles were synthesized through a wet chemical route (Sneed et al., 2014). The specific activity of Pd-Ni-Pt catalysts for MOR is four times than that of Pd/Pt catalysts. Although various core-shell structured nanocatalysts have been synthesized for MOR of fuel cells, it is still an enormous challenge to develop Pt-based core-shell structured nanoparticles with lower cost, high chemical stability. The electrocatalytic activity and stability of Pt nanoparticles can be further increased by alloying with non-noble metals such as Ni, Fe, and Cu (Ramírez-Caballero et al., 2010; Wang et al., 2011; Zhao et al., 2015). Therefore, it is a challenge to develop a facile method for preparation of high performance and high stability core-shell catalysts with Pt-based alloy. Among these transition metals, Mo has good poisoning tolerance toward MOR at room temperature. Shubina and Koper (2002) verified that the adsorption capacity of CO on PtMo bimetallic surface was weaker than that on pure Pt surface through Density Functional Theory (DFT). However, due to the large negative redox potential of Mo<sup>2+</sup>/Mo couple and the low miscibility of Pt and Mo, it is a very challenging subject to prepare PtMo alloy nanoparticles with small size by using solution-based methods (Liu et al., 2009). In this work, a reverse microemulsion (RME) method is developed to prepare core-shell structured Pt<sub>x</sub>Mo<sub>y</sub>@TiO<sub>2</sub> nanoparticles. The morphologies, particle size, structure, composition, and performance of Pt<sub>x</sub>Mo<sub>y</sub>@TiO<sub>2</sub> nanoparticles are investigated in this work. The experimental results show that Pt<sub>x</sub>Mo<sub>y</sub>@TiO<sub>2</sub> electrocatalysts possess excellent electrocatalytic activity and durability toward MOR.

## EXPERIMENT

### Materials

Molybdenum chloride (MoCl<sub>5</sub>, 99.6%), titanium isopropoxide (TiIPO, 96%), isopropanol (C<sub>3</sub>H<sub>8</sub>, 97%), n-heptane (C<sub>7</sub>H<sub>16</sub>,

98.5%), polyoxyethylene (4) lauryl ether (Brij® L4, Mn~362), ammonium hydroxide solution (NH<sub>3</sub> · H<sub>2</sub>O, 25~28%), chloroplatinic acid (H<sub>2</sub>PtCl<sub>6</sub> · 6H<sub>2</sub>O, 99.9%), tetraethyl orthosilicate (TEOS, 28.4%), methyl alcohol (CH<sub>3</sub>OH, 99.5%), acetone (C<sub>3</sub>H<sub>6</sub>O, 99.5%), hydrofluoric acid (HF, 40%), Nafion solution (5% in isopropanol and water) were purchased from AiKe reagent without further treatment.

### Synthesis of Pt<sub>x</sub>Mo<sub>y</sub>@TiO<sub>2</sub> Nanoparticles

The Pt<sub>x</sub>Mo<sub>y</sub>@TiO<sub>2</sub> nanoparticles were synthesized by referencing a previously modified method which was reported by Sean T. (Hunt et al., 2016a). In a typical synthesis process, 8 mL C<sub>12</sub>H<sub>28</sub>O<sub>4</sub>Ti and 4 mL MoCl<sub>5</sub> were added into the mixed solutions with 120 mL C<sub>7</sub>H<sub>16</sub> and 55 mL Brij® L4, which formed the transition metal precursor alcohol solution. A certain amount of H<sub>2</sub>PtCl<sub>6</sub> · 6H<sub>2</sub>O aqueous solution with 45 mL C<sub>7</sub>H<sub>16</sub> and 7.5 mL Brij® L4 were injected into the above solution drop by drop. After stirring the mixture for 4.2 h, 1.0 mL TEOS was added quickly. After 16.5 h, 300 mL methanol was added and stirred for 15 min, then lay up for 1 h at least. The white precipitate was collected by centrifugal, washed with acetone and dried under vacuum at 60°C overnight. Then white powders were heated at a rate of 2°C min<sup>-1</sup> to 870°C and maintained for 300 min under 120 cm<sup>3</sup> min<sup>-1</sup> of H<sub>2</sub> and 30 cm<sup>3</sup> min<sup>-1</sup> of CH<sub>4</sub>, then the SiO<sub>2</sub>@Pt<sub>x</sub>Mo<sub>y</sub>@TiO<sub>2</sub> nanoparticles were obtained. After slowly cooling to room temperature, the SiO<sub>2</sub>@Pt<sub>x</sub>Mo<sub>y</sub>@TiO<sub>2</sub> nanoparticles were etched by HF and ethanol for 15 h to remove the SiO<sub>2</sub> outer shell. Finally, the Pt<sub>x</sub>Mo<sub>y</sub>@TiO<sub>2</sub> nanoparticles were collected by centrifugation and washed with ethanol and water and dried under vacuum at 60°C overnight.

### Characterization

The phase of nanoparticles was characterized by X-ray Diffraction (XRD) using Cu Kα radiation. The diffraction patterns were stored from 2θ = 10–90° with a scan rate of 5° s<sup>-1</sup>. The surface composition and structure of as-prepared catalysts under ultra-high vacuum were characterized by X-ray photoelectron spectroscopy (XPS) with a monochromatic Al X-ray source (Al-KR, 1486.8 eV). All spectra were corrected by referencing the adventitious C 1s signal to 284.7 eV. The morphology and size of nanoparticles were characterized under instrument operating at 200 kV by Transmission Electron Microscopy (TEM). The samples were dispersed in acetone solution, dropped into copper TEM grids with carbon

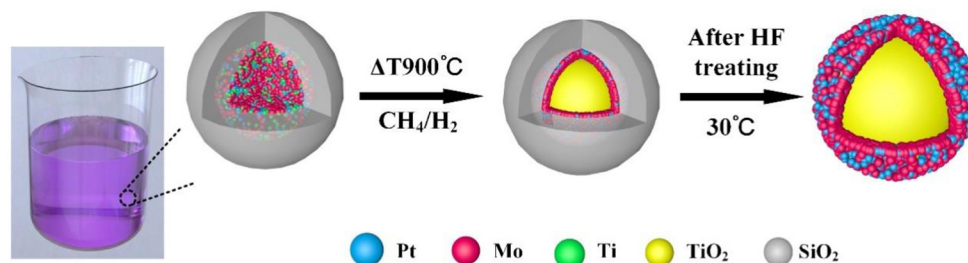


**FIGURE 1** | Schematic diagram of the synthesis of Pt<sub>x</sub>Mo<sub>y</sub>@TiO<sub>2</sub> nanoparticles.

film, cooled to room temperature. The composition of the nanoparticles was analyzed by an energy-dispersive X-ray (EDX) spectroscopy attached to the TEM.

Electrochemical measurements were carried out by using a common three-electrode cell method on the Autolab (Metrohm, PGSTAT 302N) instrument at room temperature. A glassy carbon electrode (GCE) with a diameter of 5 mm was used as the working electrode (WE), a 10×20 mm<sup>2</sup> platinum sheet was used as the counter electrode, and a silver chloride was used as the reference electrode (Ag/AgCl). Catalyst inks consisted of 10 mg Pt<sub>x</sub>Mo<sub>y</sub>@TiO<sub>2</sub> nanoparticles and 2 mL, 0.5% Nafion/isopropanol, which was treated by ultrasound for 30 min. Finally, 10 μL catalyst inks were dropped on the GCE surface and dried in air at room temperature.

## RESULTS AND DISCUSSION

Core-shell structured Pt<sub>x</sub>Mo<sub>y</sub>@TiO<sub>2</sub> nanoparticles are obtained by using the RME method. The synthesis procedure is described in **Figure 1**. First, the precursor structure is formed through the RME process. The resulting composite particles are subjected to a high-temperature reduction process, wherein the SiO<sub>2</sub> coating serves as a hard template to prevent nanoparticles sintering. Finally, core-shell structured Pt<sub>x</sub>Mo<sub>y</sub>@TiO<sub>2</sub> nanoparticles are obtained by dissolving the SiO<sub>2</sub> shell using an aqueous HF solution.

After high temperature sintering, TEM images of SiO<sub>2</sub>@Pt<sub>x</sub>Mo<sub>y</sub>@TiO<sub>2</sub> nanoparticles are shown in **Figure 2**. The images were mared with yellow dotted line to clarify the different parts for shell and core. The dark dot in the center represents the Pt<sub>x</sub>Mo<sub>y</sub>@TiO<sub>2</sub> core and the light shadow in the outer represents the SiO<sub>2</sub> shell. It can be found that all the dark dots are coated with thick shells. And the Pt<sub>x</sub>Mo<sub>y</sub>@TiO<sub>2</sub> nanospheres in the core show uniform distribution without obvious agglomeration.

The crystal structures of SiO<sub>2</sub>@Pt<sub>x</sub>Mo<sub>y</sub>@TiO<sub>2</sub> and ETEK nanoparticles are characterized by the XRD pattern. As shown

in **Figure 3**, the diffraction peaks of SiO<sub>2</sub> (PDF#01-082-0512) are located at 21.8, 35.9, and 69.0°. A set of diffraction peaks for TiO<sub>2</sub> at 2θ of 27.4, 41.2, 44.0, 54.3, and 56.6° indicate the existence of TiO<sub>2</sub> (PDF#01-086-0147) in the compounds. The diffraction peaks of PtMo alloy (PDF#03-065-5035) are located at 39.93, 46.43, 67.78, and 81.65°. Each of them corresponds to a crystal face, which is (111), (200), (220), and (311) facets of face-centered cubic (fcc) structure (Chen and Pan, 2009; Zhang et al., 2019). Because the content of PtMo is much lower than TiO<sub>2</sub> and SiO<sub>2</sub>, the intensities of PtMo diffraction peaks are much lower than TiO<sub>2</sub> and SiO<sub>2</sub>.

The morphology and composition of the Pt<sub>x</sub>Mo<sub>y</sub>@TiO<sub>2</sub> nanoparticles without silica shell are further characterized by TEM combined with EDX, as shown in **Figure 4**. The nanoparticle sizes of Pt<sub>0.5</sub>Mo<sub>0.5</sub>@TiO<sub>2</sub>, Pt<sub>0.25</sub>Mo<sub>0.75</sub>@TiO<sub>2</sub>, and Pt<sub>0.2</sub>Mo<sub>0.8</sub>@TiO<sub>2</sub> are all about 12~15 nm with uniform

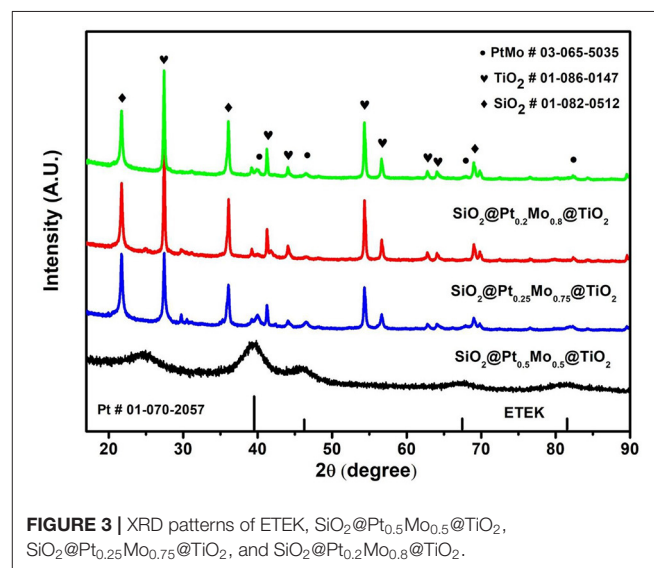


**FIGURE 3** | XRD patterns of ETEK, SiO<sub>2</sub>@Pt<sub>0.5</sub>Mo<sub>0.5</sub>@TiO<sub>2</sub>, SiO<sub>2</sub>@Pt<sub>0.25</sub>Mo<sub>0.75</sub>@TiO<sub>2</sub>, and SiO<sub>2</sub>@Pt<sub>0.2</sub>Mo<sub>0.8</sub>@TiO<sub>2</sub>.

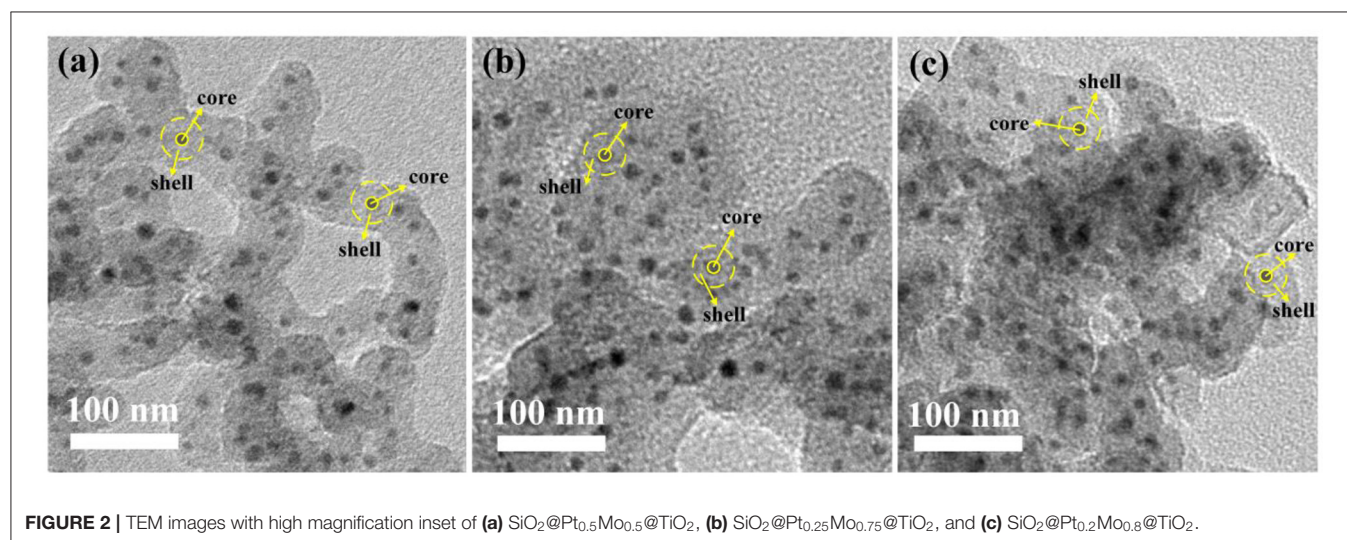


**FIGURE 2** | TEM images with high magnification inset of (a) SiO<sub>2</sub>@Pt<sub>0.5</sub>Mo<sub>0.5</sub>@TiO<sub>2</sub>, (b) SiO<sub>2</sub>@Pt<sub>0.25</sub>Mo<sub>0.75</sub>@TiO<sub>2</sub>, and (c) SiO<sub>2</sub>@Pt<sub>0.2</sub>Mo<sub>0.8</sub>@TiO<sub>2</sub>.

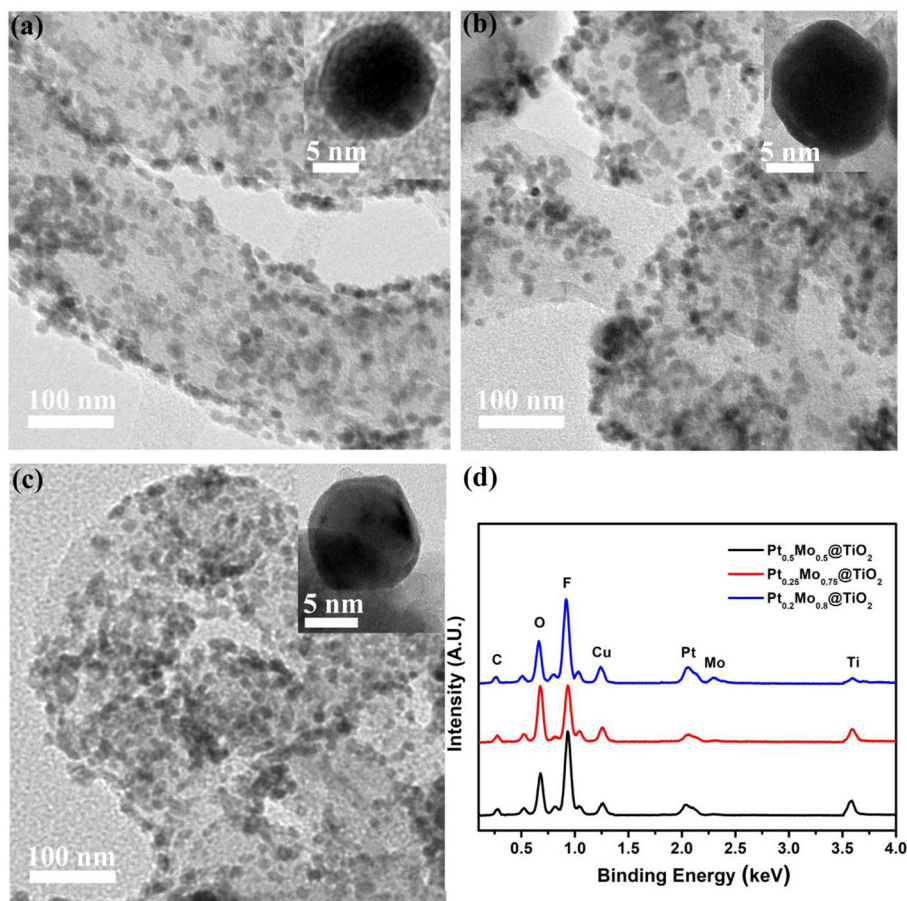


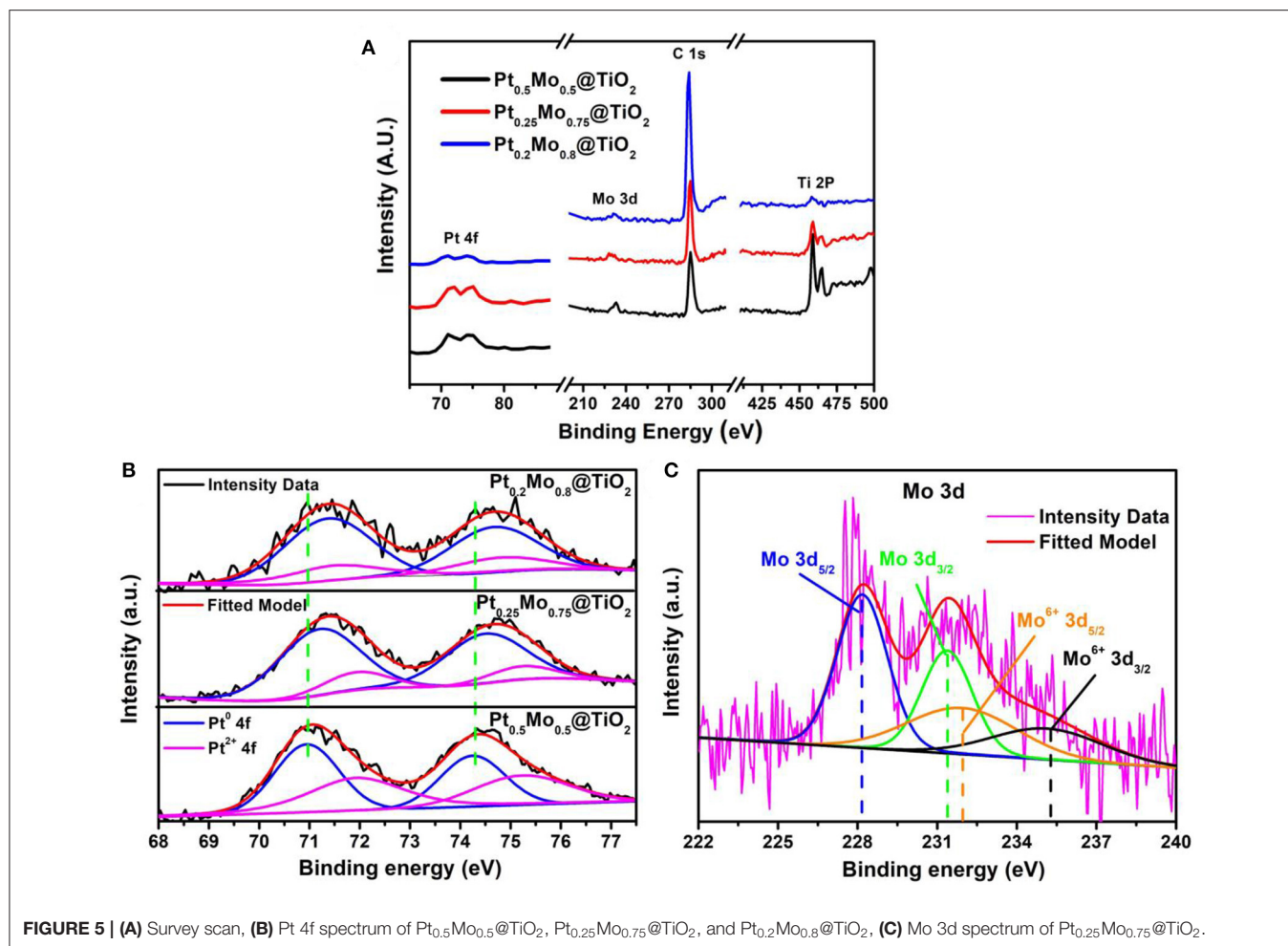
**FIGURE 4** | TEM images with high magnification inset of (a) Pt<sub>0.5</sub>Mo<sub>0.5</sub>@TiO<sub>2</sub>, (b) Pt<sub>0.25</sub>Mo<sub>0.75</sub>@TiO<sub>2</sub> and (c) Pt<sub>0.2</sub>Mo<sub>0.8</sub>@TiO<sub>2</sub>, and (d) the corresponding EDX spectra.

distribution. Inset high magnification pictures clearly show that PtMo alloy is uniformly coated with TiO<sub>2</sub>. The EDX spectra results of different nanoparticle components are shown in **Figure 4d**. The EDX images show that the existence of Pt, Mo and Ti elements, and the intensity of Mo peak increases with increasing the Mo content in the precursor solution. The existence of Cu elements comes from the copper mesh used in the preparation of TEM samples.

The surface element composition and chemical state of Pt<sub>x</sub>Mo<sub>y</sub>@TiO<sub>2</sub> nanoparticles are further investigated by XPS measurements. It can be found that three elements of Pt, Mo, and Ti exist in XPS survey, as shown in **Figure 5A**. The Pt 4f region of the Pt<sub>x</sub>Mo<sub>y</sub>@TiO<sub>2</sub> samples can be divided into two pairs of doublets, as shown in **Figure 5B**. The Pt<sub>0.5</sub>Mo<sub>0.5</sub>@TiO<sub>2</sub> nanoparticles exhibit a pair of Pt 4f<sub>7/2</sub> signal centered at 71.0 and 74.3 eV, which is consistent with the metallic Pt (Cao et al., 2013; Hunt et al., 2016b). The weak doublet peaks at 72.1 and 75.4 eV can be assigned to the Pt oxides (Tang et al., 2018). The Pt<sub>0.25</sub>Mo<sub>0.75</sub>@TiO<sub>2</sub> and Pt<sub>0.2</sub>Mo<sub>0.8</sub>@TiO<sub>2</sub> also show two doublet peaks that can be associated with metallic Pt and Pt oxides. Obviously, a pair of peaks at 71.2 and 74.5 eV are associated

with the metallic Pt of Pt<sub>0.25</sub>Mo<sub>0.75</sub>@TiO<sub>2</sub>, another pair of peaks at 71.4 and 74.7 eV are associated with the metallic Pt of Pt<sub>0.2</sub>Mo<sub>0.8</sub>@TiO<sub>2</sub>. Compared with Pt<sub>0.2</sub>Mo<sub>0.8</sub>@TiO<sub>2</sub> samples, a large negative shift in Pt 4f<sub>7/2</sub> binding energy is observed in Pt<sub>0.5</sub>Mo<sub>0.5</sub>@TiO<sub>2</sub> and Pt<sub>0.25</sub>Mo<sub>0.75</sub>@TiO<sub>2</sub> samples, which can weaken the Pt-CO<sub>ads</sub> and promote the C-H cleavage on Pt sites (StamenkovIc et al., 2007; Stephens et al., 2011; Dubau et al., 2015). **Figure 5C** shows the Mo 3d spectra of the Pt<sub>0.5</sub>Mo<sub>0.5</sub>@TiO<sub>2</sub> sample. The results show that the strong double peaks at 228.2 and 231.4 eV can be assigned to metallic Mo, the weak doublet peaks at 231.7 and 234.9 eV can be assigned to the Mo oxides. This indicates that Mo exists in the form of PtMo alloy in the Pt<sub>0.25</sub>Mo<sub>0.75</sub>@TiO<sub>2</sub> samples, which is consistent with the XRD results.

The electrocatalytic activities of ETEK, Pt<sub>0.5</sub>Mo<sub>0.5</sub>@TiO<sub>2</sub>, Pt<sub>0.25</sub>Mo<sub>0.75</sub>@TiO<sub>2</sub>, and Pt<sub>0.2</sub>Mo<sub>0.8</sub>@TiO<sub>2</sub> electrocatalysts are examined at room temperature in N<sub>2</sub>-saturated 0.5 M H<sub>2</sub>SO<sub>4</sub> with or without 1.0 M CH<sub>3</sub>OH solutions, as shown in **Figure 6**. The electrochemical surface area (ECSA) is an



important parameter, which is usually measured by the hydrogen adsorption/desorption area in the cyclic voltammograms (CV) curves and assumed to be  $210 \mu\text{C cm}^{-2}$  for the adsorption of a hydrogen monolayer (Lim et al., 2009). The typical CV of different electrocatalysts in 0.5 M H<sub>2</sub>SO<sub>4</sub> solution are displayed in **Figure 6A**. The scan rate is  $50 \text{ mV s}^{-1}$  in the potential range of  $-0.2$ – $1.0$  V. The comparison of ECSA between ETEK and as-prepared electrocatalysts is shown in **Figure 6A** and the corresponding electrochemical parameters are shown in **Table 1**. The Pt<sub>0.25</sub>Mo<sub>0.75</sub>@TiO<sub>2</sub> electrocatalyst has a higher ECSA ( $593.9 \text{ cm}^2 \text{ mg}_{\text{Pt}}^{-1}$ ), about 3.1 times higher than that of ETEK ( $193.3 \text{ cm}^2 \text{ mg}_{\text{Pt}}^{-1}$ ). The high active surface area of Pt<sub>0.25</sub>Mo<sub>0.75</sub>@TiO<sub>2</sub> is attributed to the small size and the synergistic effect between Pt and Mo. Higher ECSA tends to provide more active sites for hydrogen adsorption/desorption, which is very favorable for MOR.

A negative onset potential and a higher peak current density of MOR are also needed for a good catalyst (Lu et al., 2012). As shown in **Figure 6B**, the onset potential of the Pt<sub>0.25</sub>Mo<sub>0.75</sub>@TiO<sub>2</sub> catalyst for MOR is 0.12 V, which is more negative than that of ETEK (0.23 V). The results indicate that MOR can occur more easily on the Pt<sub>0.25</sub>Mo<sub>0.75</sub>@TiO<sub>2</sub> than

on the ETEK. To gain further insights into the activities of different catalysts, the electrocatalytic activities of ETEK, Pt<sub>0.5</sub>Mo<sub>0.5</sub>@TiO<sub>2</sub>, Pt<sub>0.25</sub>Mo<sub>0.75</sub>@TiO<sub>2</sub>, and Pt<sub>0.2</sub>Mo<sub>0.8</sub>@TiO<sub>2</sub> electrocatalysts for MOR in N<sub>2</sub>-saturated 0.5 M H<sub>2</sub>SO<sub>4</sub> with 1.0 M CH<sub>3</sub>OH solution are examined at room temperature as shown in **Figure 6B**. The test parameters of **Figure 6B** are the same as **Figure 6A**. The peak current density of ETEK for the MOR is  $449.37 \text{ mA mg}_{\text{Pt}}^{-1}$ . However, the peak current densities of Pt<sub>0.5</sub>Mo<sub>0.5</sub>@TiO<sub>2</sub>, Pt<sub>0.25</sub>Mo<sub>0.75</sub>@TiO<sub>2</sub>, and Pt<sub>0.2</sub>Mo<sub>0.8</sub>@TiO<sub>2</sub> samples for the MOR are 1.2 times ( $540.34 \text{ mA mg}_{\text{Pt}}^{-1}$ ), 1.3 times ( $583.86 \text{ mA mg}_{\text{Pt}}^{-1}$ ), and 1.5 times ( $515.47 \text{ mA mg}_{\text{Pt}}^{-1}$ ) than that of ETEK. The improvement of catalyst activity is due to the alloying effect of PtMo, which results in the shift of the d-band center of the surface Pt atoms and the increase of MOR activity (Han et al., 2015).

The  $I_f/I_b$  ratio represents the tolerance of CO on the platinum surface, in which  $I_f$  is the forward peak current and  $I_b$  is the reverse peak current (Hassan et al., 2015). The  $I_f/I_b$  values of the Pt<sub>0.5</sub>Mo<sub>0.5</sub>@TiO<sub>2</sub>, Pt<sub>0.25</sub>Mo<sub>0.75</sub>@TiO<sub>2</sub>, Pt<sub>0.2</sub>Mo<sub>0.8</sub>@TiO<sub>2</sub>, and ETEK are calculated to be 1.01, 1.00, 0.97, and 0.86, respectively (**Table 1**), implying that the Pt<sub>x</sub>Mo<sub>y</sub>@TiO<sub>2</sub> electrocatalysts have a high tolerance to CO poisoning species. The anti-poisoning of

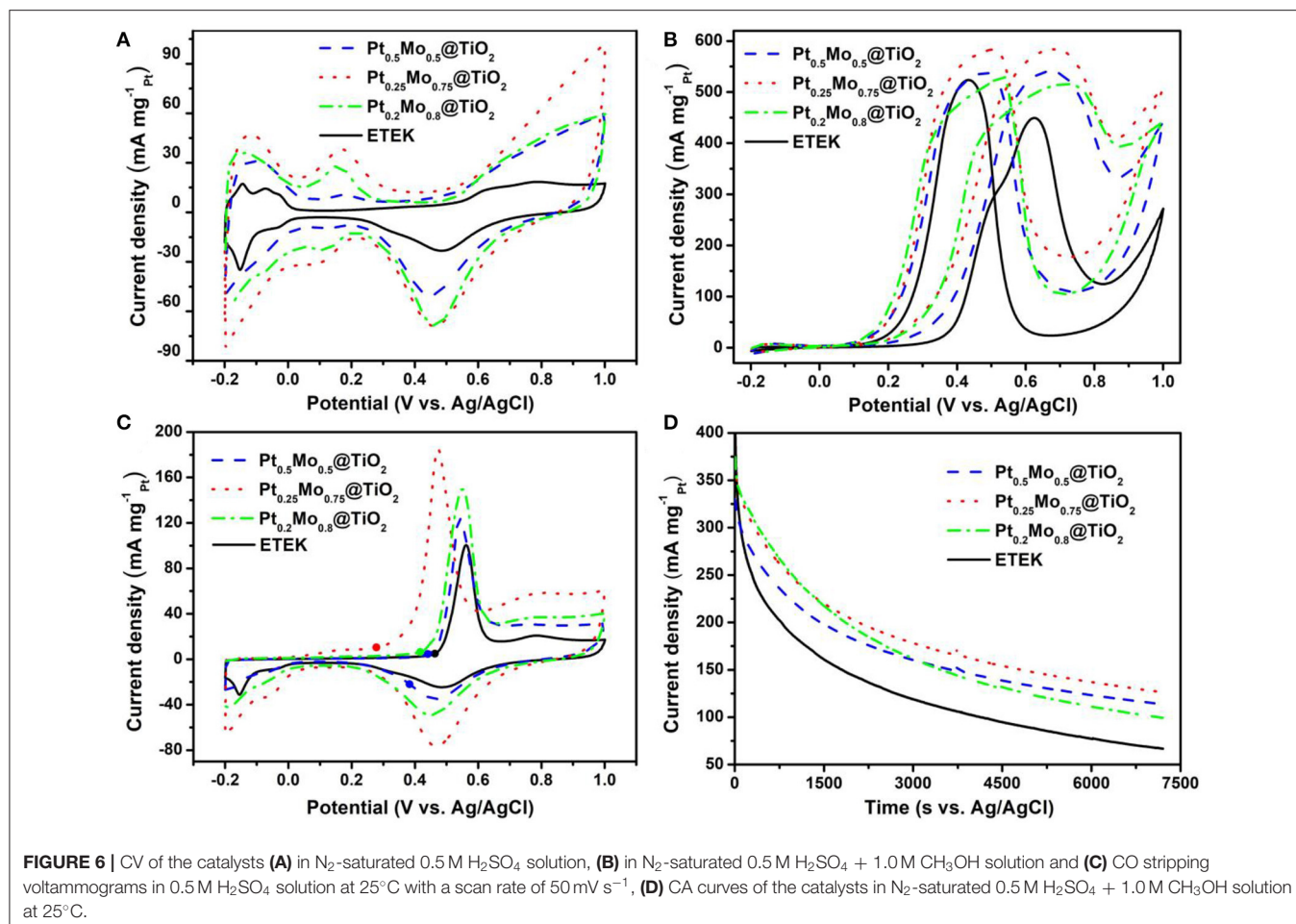
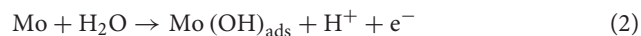


**FIGURE 6** | CV of the catalysts **(A)** in N<sub>2</sub>-saturated 0.5 M H<sub>2</sub>SO<sub>4</sub> solution, **(B)** in N<sub>2</sub>-saturated 0.5 M H<sub>2</sub>SO<sub>4</sub> + 1.0 M CH<sub>3</sub>OH solution and **(C)** CO stripping voltammograms in 0.5 M H<sub>2</sub>SO<sub>4</sub> solution at 25°C with a scan rate of 50 mV s<sup>-1</sup>, **(D)** CA curves of the catalysts in N<sub>2</sub>-saturated 0.5 M H<sub>2</sub>SO<sub>4</sub> + 1.0 M CH<sub>3</sub>OH solution at 25°C.

**TABLE 1** | The properties and electrochemical parameters of the different catalysts.

Catalysts	ECSA (cm <sup>2</sup> mg <sub>Pt</sub> <sup>-1</sup> )	Onset potential (V)	Peak potential (V)	Peak current (mA mg <sub>Pt</sub> <sup>-1</sup> )	Ratio ( <i>I<sub>f</sub></i> / <i>I<sub>b</sub></i> )
ETEK	193.3	0.23	0.63	449.37	0.86
Pt <sub>0.5</sub> Mo <sub>0.5</sub> @TiO <sub>2</sub>	275.2	0.11	0.64	540.34	1.01
Pt <sub>0.25</sub> Mo <sub>0.75</sub> @TiO <sub>2</sub>	593.9	0.12	0.68	583.86	1.00
Pt <sub>0.2</sub> Mo <sub>0.8</sub> @TiO <sub>2</sub>	471.6	0.18	0.7	515.74	0.97

CO is further demonstrated by CO stripping voltammograms in 0.5 M H<sub>2</sub>SO<sub>4</sub> solution at 25°C with a scan rate of 50 mV s<sup>-1</sup>. As shown in **Figure 6C**, the onset potentials of Pt<sub>0.5</sub>Mo<sub>0.5</sub>@TiO<sub>2</sub>, Pt<sub>0.25</sub>Mo<sub>0.75</sub>@TiO<sub>2</sub>, and Pt<sub>0.2</sub>Mo<sub>0.8</sub>@TiO<sub>2</sub> are 0.28, 0.39, and 0.44 V. However, the onset potential of ETEK is 0.46 V, illustrating that the pre-adsorbed CO on Pt<sub>0.5</sub>Mo<sub>0.5</sub>@TiO<sub>2</sub> and Pt<sub>0.25</sub>Mo<sub>0.75</sub>@TiO<sub>2</sub> catalysts is easier to be oxidized than that on ETEK. The bi-functional mechanism could further explain the resisted CO poisoning of Pt<sub>x</sub>Mo<sub>y</sub>@TiO<sub>2</sub> electrocatalyst in theory. The bi-functional mechanism could be summarized as follows (Levy and Boudart, 1973; Wang et al., 2006; Lu et al., 2016):

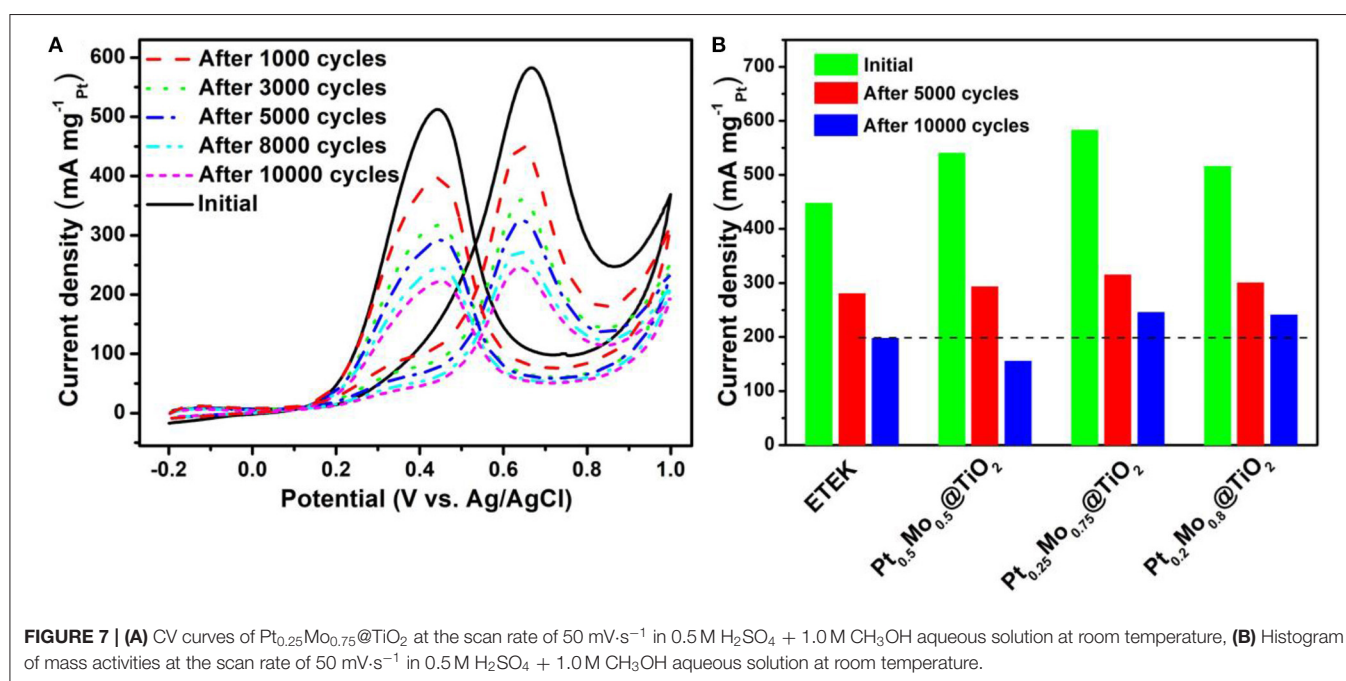


Mo can activate the interfacial water and generate OH species at low potential to facilitate the oxidation of intermediates species, such as CO<sub>ad</sub>, which is evidenced by the CO<sub>ad</sub> stripping voltammograms. The electrocatalytic stabilities of Pt<sub>0.5</sub>Mo<sub>0.5</sub>@TiO<sub>2</sub>, Pt<sub>0.25</sub>Mo<sub>0.75</sub>@TiO<sub>2</sub>, Pt<sub>0.2</sub>Mo<sub>0.8</sub>@TiO<sub>2</sub>, and ETEK were tested under 0.6 V for 7200 s in N<sub>2</sub>-saturated 0.5 M H<sub>2</sub>SO<sub>4</sub> solution containing 1.0 M CH<sub>3</sub>OH solutions, as shown in **Figure 6D**. In the early stage, the current density decreases sharply because the electrocatalyst surfaces are poisoned (Wang et al., 2014; Jin et al., 2020). As time goes by, the current decreases slowly. After 7200 s, the current of pre-prepared electrocatalyst is also higher than that of commercial ETEK. The polarization currents of Pt<sub>0.5</sub>Mo<sub>0.5</sub>@TiO<sub>2</sub>, Pt<sub>0.25</sub>Mo<sub>0.75</sub>@TiO<sub>2</sub>, and Pt<sub>0.2</sub>Mo<sub>0.8</sub>@TiO<sub>2</sub> are 113.8, 126.4, and 99.5 mA mg<sub>Pt</sub><sup>-1</sup>, respectively, but ETEK is only 66.8 mA mg<sub>Pt</sub><sup>-1</sup>.

The comparisons between some papers published recently and this work are tabled in **Table 2**. It can be seen clearly that the

**TABLE 2** | Comparisons of the MOR performance for Pt based catalysts in recently published papers.

References	Catalyst	ECSA (cm <sup>2</sup> mg <sub>Pt</sub> <sup>-1</sup> )	Electrolyte	Mass activity (mA mg <sub>Pt</sub> <sup>-1</sup> )	Methods
Zhu et al. (2014)	Pt/NC <sub>x</sub> -TiO <sub>2</sub> -2	—	0.5 M H <sub>2</sub> SO <sub>4</sub> +1.0 M CH <sub>3</sub> OH	382.2	Microwave-assisted method
Tang et al. (2018)	PtNiCu ERDS	615	0.5 M H <sub>2</sub> SO <sub>4</sub> +1.0 M CH <sub>3</sub> OH	—	One-pot method
Lu et al. (2012)	Pt/WC/C <sub>10</sub>	423.6	0.5 M H <sub>2</sub> SO <sub>4</sub> +1.0 M CH <sub>3</sub> OH	313	Improved impregnation method
Levy and Boudart (1973)	Pt@WC/OMC	—	0.5 M H <sub>2</sub> SO <sub>4</sub> +1.0 M CH <sub>3</sub> OH	367.5	Pulse-microwave polyol method
Wang et al. (2006)	Pt/TiO <sub>2</sub> @NC-NCTs-7	826	0.5 M H <sub>2</sub> SO <sub>4</sub> +1.0 M CH <sub>3</sub> OH	577	Solvent heating method
This work	Pt <sub>0.25</sub> Mo <sub>0.75</sub> @TiO <sub>2</sub>	593.5	0.5 M H <sub>2</sub> SO <sub>4</sub> +1.0 M CH <sub>3</sub> OH	583.86	Reverse microemulsion method



Pt<sub>0.25</sub>Mo<sub>0.75</sub>@TiO<sub>2</sub> electrocatalyst in this work shows the highest mass activity for MOR in the similar testing conditions.

The durability tests are carried out by sweeping the potential from  $-0.2$  V to  $1.0$  V (vs. Ag/AgCl) for 10,000 cycles at a sweep rate of  $50$  mV s<sup>-1</sup> as shown in Figure 7. It can be seen clearly that the current density decreases and the onset potential shifts positively with increasing the scan cycles in Figure 7A. As can be seen from Figure 7B, the mass activities of ETEK, Pt<sub>0.5</sub>Mo<sub>0.5</sub>@TiO<sub>2</sub>, Pt<sub>0.25</sub>Mo<sub>0.75</sub>@TiO<sub>2</sub>, and Pt<sub>0.2</sub>Mo<sub>0.8</sub>@TiO<sub>2</sub> decrease respectively to 55.6, 72.5, 57.3, and 53.8% after 10,000 cycles. Compared to the commercial Pt/C (ETEK), the Pt<sub>0.25</sub>Mo<sub>0.75</sub>@TiO<sub>2</sub> electrocatalyst still demonstrates significantly higher electrocatalytic activity after the longtime test. The highest stability and catalyst activity of Pt<sub>x</sub>Mo<sub>y</sub>@TiO<sub>2</sub> electrocatalysts can be attributed to the unique core-shell structure and the uniform coating of PtMo alloy on the surface

of acid-resistant TiO<sub>2</sub>. On the other hand, TiO<sub>2</sub> has stronger corrosion resistance in acidic medium than carbon support, which can enhance the durability of catalyst. And TiO<sub>2</sub> as support may modify the surface electronic structure of Pt, resulting in the enhanced electrocatalytic activity.

## CONCLUSION

In summary, Pt<sub>x</sub>Mo<sub>y</sub>@TiO<sub>2</sub> nanoparticles with core-shell structure are prepared successfully using the RME method. The Pt<sub>x</sub>Mo<sub>y</sub>@TiO<sub>2</sub> nanoparticles composed of acid-resistant TiO<sub>2</sub> core with thin layer PtMo alloy shell. The component of the Pt<sub>x</sub>Mo<sub>y</sub>@TiO<sub>2</sub> nanoparticles can be tuned by adjusting reactant concentrations. The Pt<sub>x</sub>Mo<sub>y</sub>@TiO<sub>2</sub> electrocatalyst exhibits higher catalytic activity and stability for MOR

performance relative to the commercial ETEK. Especially, the Pt<sub>0.25</sub>Mo<sub>0.75</sub>@TiO<sub>2</sub> electrocatalyst has an excellent MOR performance. The high MOR activity is attributed to the unique core-shell structure, which can enhance the utilization rate of Pt and provide more active sites. In addition, the alloying effect of Pt and Mo can cause the shift of the d-band center of Pt atoms and increase the MOR activity. A feasible strategy for preparing core-shell structured nanoparticles is developed in this work. The research results may be beneficial to the further development of the electrocatalyst industry.

## DATA AVAILABILITY STATEMENT

The original contributions presented in the study are included in the article/Supplementary Material, further inquiries can be directed to the corresponding author.

## REFERENCES

- Cao, C. L., Hu, C. G., Tian, J., Shen, W. D., Wang, S. X., and Liu, H. (2013). Pt nanoparticles supported inside TiO<sub>2</sub> nanotubes for effective ethanol electrooxidation. *J. Electrochem. Soc.* 160, H793–H799. doi: 10.1149/2.011311jes
- Chen, C. S., and Pan, F. M. (2009). Electrocatalytic activity of Pt nanoparticles deposited on porous TiO<sub>2</sub> supports toward methanol oxidation. *Appl. Catal. B Environ.* 91, 663–669. doi: 10.1016/j.apcatb.2009.07.008
- Dubau, L., Asset, T., Chattot, R., Bonnaud, C., Vanpeene, V., Nelayah, J., et al. (2015). Tuning the performance and the stability of porous hollow PtNi/C nanostructures for the oxygen reduction reaction. *ACS Catal.* 5, 5333–5341. doi: 10.1021/acscatal.5b01248
- Han, L., Li, X. R., Ma, J., Yu, Y., and Lu, J. L. (2015). An in-situ synthesized PEDOT:PSS/TiO<sub>2</sub> nanocomposite film by electropolymerization and its enhanced electrochromic properties. *Nanosci. Nanotech. Lett.* 7, 308–313. doi: 10.1166/nml.2015.1918
- Hassan, A., Paganin, V. A., and Ticianelli, E. A. (2015). Pt modified tungsten carbide as anode electrocatalyst for hydrogen oxidation in proton exchange membrane fuel cell: CO tolerance and stability. *Appl. Catal. B Environ.* 165, 611–619. doi: 10.1016/j.apcatb.2014.10.068
- Hunt, S. T., Milina, M., Alba-Rubio, A. C., Hendon, C. H., Dumesic, J. A., and Roman-Leshkov, Y. (2016a). Self-assembly of noble metal monolayers on transition metal carbide nanoparticle catalysts. *Science* 352, 974–978. doi: 10.1126/science.aad8471
- Hunt, S. T., Milina, M., Wang, Z. S., and Roman-Leshkov, Y. (2016b). Activating earth-abundant electrocatalysts for efficient, low-cost hydrogen evolution/oxidation: sub-monolayer platinum coatings on titanium tungsten carbide nanoparticles. *Energ. Environ. Sci.* 9, 3290–3301. doi: 10.1039/C6EE01929C
- Jin, M., Lu, S. Y., Zhong, X. J., Liu, H., Liu, H., Gan, M. Y., et al. (2020). Spindle-like MOF derived TiO<sub>2</sub>@NC-NCNTs composite with modulating defect site and graphitization nanoconfined Pt NPs as superior bifunctional fuel cell electrocatalysts. *ACS Sustain. Chem. Eng.* 8, 1933–1942. doi: 10.1021/acssuschemeng.9b06329
- Kwon, T., Jun, M., Kim, H. Y., Oh, A., Park, J., Baik, H., et al. (2018). Vertex-reinforced PtCuCo ternary nanoframes as efficient and stable electrocatalysts for the oxygen reduction reaction and the ethanol oxidation reaction. *Adv. Funct. Mater.* 28, 1706440–1706449. doi: 10.1002/adfm.201706440
- Lang, X. L., Shi, M. Q., Jiang, Y. K., Chen, H., and Ma, C. N. (2016). Tungsten carbide/porous carbon core-shell nanocomposites as a catalyst support for methanol oxidation. *RSC Adv.* 6, 13873–13880. doi: 10.1039/C5RA18817B
- Levy, R. B., and Boudart, M. (1973). Platinum-like behavior of tungsten carbide in surface catalysis. *Science* 181, 547–549. doi: 10.1126/science.181.4099.547

## AUTHOR CONTRIBUTIONS

TA: conceptualization, methodology, data curation, formal analysis, resources, visualization, and writing-original draft preparation. SB: validation. JL: investigation, supervision, writing-reviewing and editing, project administration, and funding acquisition. All authors contributed to the article and approved the submitted version.

## FUNDING

This work was supported by the National Natural Science Foundation of China (51774177, 52004121), the University of Science and Technology Liaoning Talent Grant (601010324), Program of Distinguished Professor of Liaoning Province (2017-60).

- Li, C. L., and Yamauchi, Y. (2013). Facile solution synthesis of Ag@Pt core-shell nanoparticles with dendritic Pt shells. *Phys. Chem. Chem. Phys.* 15, 3490–3496. doi: 10.1039/c3cp44313b
- Lim, B., Jiang, M. J., Camargo, P. H. C., Cho, E. C., Tao, J., Liu, X. M., et al. (2009). Pd-Pt bimetallic nanodendrites with high activity for oxygen reduction. *Science* 324, 1302–1305. doi: 10.1126/science.1170377
- Lin, Z. Y., Guo, X. W., Wang, Z. C., Wang, B. Y., He, S. H., O'Dell, L. A., et al. (2020). A wide-temperature superior ionic conductive polymer electrolyte for lithium metal battery. *Nano Energy* 73, 104786–104794. doi: 10.1016/j.nanoen.2020.104786
- Liu, J., Lan, J. Z., Yang, L. Y., Wang, F., and Jiao, Y. (2019). PtM(FeCoNi) bimetallic nanoclusters as active, methanol tolerant, and stable catalysts toward the oxygen reduction reaction. *ACS Sustain. Chem. Eng.* 7, 6541–6549. doi: 10.1021/acssuschemeng.8b04929
- Liu, Z. F., Hu, J. E., Wang, Q., Gaskell, K., Frenkel, A. I., Jackson, G. S., et al. (2009). PtMo alloy and MoO<sub>x</sub>@Pt core-shell nanoparticles as highly CO-tolerant electrocatalysts. *J. Am. Chem. Soc.* 131, 6924–6925. doi: 10.1021/ja901303d
- Lu, J. L., Li, Z. H., Jiang, S. P., Shen, P. K., and Li, L. (2012). Nanostructured tungsten carbide/carbon composites synthesized by a microwave heating method as supports of platinum catalysts for methanol oxidation. *J. Power Sources* 202, 56–62. doi: 10.1016/j.jpowsour.2011.11.018
- Lu, S. L., Eid, K., Lin, M., Wang, L., Wang, H. J., and Gu, H. W. (2016). Hydrogen gas-assisted synthesis of worm-like PtMo wavy nanowires as efficient catalysts for the methanol oxidation reaction. *J. Mater. Chem. A* 4, 10508–10513. doi: 10.1039/C6TA02053D
- Luo, J., Wang, L. Y., Mott, D., Njoki, P. N., Lin, Y., He, T., et al. (2008). Core/Shell nanoparticles as electrocatalysts for fuel cell reactions. *Adv. Mater.* 20, 4342–4347. doi: 10.1002/adma.200703009
- Oh, A., Kim, H. Y., Baik, H., Kim, B., Chaudhari, N. K., Joo, S. H., et al. (2018). Topotactic transformations in an icosahedral nanocrystal to form efficient water-splitting catalysts. *Adv. Mater.* 31, 1805546–1805553. doi: 10.1002/adma.201805546
- Ramírez-Caballero, G. E., Ma, Y. G., Callejas-Tovar, R., and Balbuena, P. B. (2010). Surface segregation and stability of core-shell alloy catalysts for oxygen reduction in acid medium. *Phys. Chem. Chem. Phys.* 12, 2209–2218. doi: 10.1039/b917899f
- Shubina, T. E., and Koper, M. T. M. (2002). Quantum-chemical calculations of CO and OH interacting with bimetallic surfaces. *Electrochim. Acta* 47, 3621–3628. doi: 10.1016/S0013-4686(02)00332-8
- Sneed, B. T., Young, A. P., Jalalpoor, D., Golden, M. C., Mao, S. J., and Jiang, Y., et al. (2014). Shaped Pd-Ni-Pt core-sandwich-shell nanoparticles: influence of Ni sandwich layers on catalytic electrooxidations. *ACS Nano* 8, 7239–7250. doi: 10.1021/nn502259g
- Stamenkovic, V. R., Fowler, B., Mun, B. S., Wang, G. F., Ross, P. N., Lucas, C. A., et al. (2007). Improved oxygen reduction activity on Pt<sub>3</sub>Ni(111) via

- increased surface site availability. *Science* 315, 493–497. doi: 10.1126/science.1135941
- Stephens, I. E. L., Bondarenko, A. S., Perez-Alonso, F. J., Calle-Vallejo, F., Bech, L., Johansson, T. P., et al. (2011). Tuning the activity of Pt(111) for oxygen electroreduction by subsurface alloying. *J. Am. Chem. Soc.* 133, 5485–5491. doi: 10.1021/ja111690g
- Tang, M., Luo, S. P., Wang, K., Du, H. Y., Sripathoorat, R., and Shen, P. K. (2018). Simultaneous formation of trimetallic Pt-Ni-Cu excavated rhombic dodecahedrons with enhanced catalytic performance for the methanol oxidation reaction. *Nano Res.* 11, 4786–4795. doi: 10.1007/s12274-018-2063-3
- Wang, C., Vliet, D. V. D., More, K. L., Zaluzec, N. J., and Stamenkovic, V. R. (2011). Multimetallic AuFePt<sub>3</sub> nanoparticles as highly durable electrocatalyst. *Nano Lett.* 11, 919–926. doi: 10.1021/nl102369k
- Wang, K., Wang, Y., Liang, Z. X., Liang, Y. R., Wu, D. C., Song, S. Q., et al. (2014). Ordered mesoporous tungsten carbide/carbon composites promoted Pt catalyst with high activity and stability for methanol electrooxidation. *Appl. Catal. B Environ.* 147, 518–525. doi: 10.1016/j.apcatb.2013.09.020
- Wang, Q. M., Chen, S. G., Li, P., Ibraheem, S., Li, J., Deng, J. H., et al. (2019). Surface Ru enriched structurally ordered intermetallic PtFe@PtRuFe core-shell nanostructure boosts methanol oxidation reaction catalysis. *Appl. Catal. B Environ.* 252, 120–127. doi: 10.1016/j.apcatb.2019.04.023
- Wang, Z. B., Yin, G. P., Zhang, J., Sun, Y. C., and Shi, P. F. (2006). Co-catalytic effect of Ni in the methanol electro-oxidation on Pt-Ru/C catalyst for direct methanol fuel cell. *Electrochim. Acta* 51, 5691–5697. doi: 10.1016/j.electacta.2006.03.002
- Zhang, H., Yin, Y. J., Hu, Y. J., Li, C. Y., Wu, P., and Wei, S. H., et al. (2010). Pd@Pt core-shell nanostructures with controllable composition synthesized by a microwave method and their enhanced electrocatalytic activity toward oxygen reduction and methanol oxidation. *J. Phys. Chem. C* 114, 11861–11867. doi: 10.1021/jp101243k
- Zhang, X. W., Ai, T. Y., Ma, C., and Lu, J. L. (2019). A novel Pt/WC<sub>x</sub>/C electrocatalyst synthesized by a one-pot method for methanol electrooxidation in acid media. *Int. J. Electrochem. Sci.* 14, 10931–10942. doi: 10.20964/2019.12.28
- Zhao, X., Chen, S., Fang, Z. C., Ding, J., Sang, W., Wang, Y. C., et al. (2015). Octahedral Pd@Pt<sub>1.8</sub>Ni core-shell nanocrystals with ultrathin PtNi alloy shells as active catalysts for oxygen reduction reaction. *J. Am. Chem. Soc.* 137, 2804–2807. doi: 10.1021/ja511596c
- Zhao, X., Yin, M., Ma, L., Liang, L., Liu, C. P., Liao, J. H., et al. (2011). Recent advances in catalysts for direct methanol fuel cells. *Energy Environ. Sci.* 4, 2736–2753. doi: 10.1039/c1ee01307f
- Zhu, J. B., Zhao, X., Xiao, M. L., Liang, L., Liu, C. P., Liao, J. H., et al. (2014). The construction of nitrogen-doped graphitized carbon–TiO<sub>2</sub> composite to improve the electrocatalyst for methanol oxidation. *Carbon* 72, 114–124. doi: 10.1016/j.carbon.2014.01.062

**Conflict of Interest:** The authors declare that the research was conducted in the absence of any commercial or financial relationships that could be construed as a potential conflict of interest.

Copyright © 2021 Ai, Bao and Lu. This is an open-access article distributed under the terms of the Creative Commons Attribution License (CC BY). The use, distribution or reproduction in other forums is permitted, provided the original author(s) and the copyright owner(s) are credited and that the original publication in this journal is cited, in accordance with accepted academic practice. No use, distribution or reproduction is permitted which does not comply with these terms.